Research Article | Vol. 26, No. 18 | 3 Sep 2018 | OPTICS EXPRESS 23844
Optics EXPRESS

Method for direct observation of Bloch oscillations in semiconductors

LIANG LI,[1] PENGFEI LAN,[1,*] XI LIU,[1] LIXIN HE,[1] XIAOSONG ZHU,[1,5] OLIVER D. MÜCKE,[2,3] PEIXIANG LU[1,4,6]

[1] *Wuhan National Laboratory for Optoelectronics and School of Physics, Huazhong University of Science and Technology, Wuhan 430074, China*
[2] *Center for Free-Electron Laser Science CFEL, Deutsches Elektronen-Synchrotron DESY, Notkestraße 85, 22607 Hamburg, Germany*
[3] *The Hamburg Centre for Ultrafast Imaging, Luruper Chaussee 149, 22761 Hamburg, Germany*
[4] *Laboratory of Optical Information Technology, Wuhan Institute of Technology, Wuhan 430205, China*
[5] *zhuxiaosong@hust.edu.cn*
[6] *lupeixiang@hust.edu.cn*
[*] *pengfeilan@hust.edu.cn*

Abstract: We propose a scheme for real-time observations of Bloch oscillations in semiconductors using time-resolved band gap emission spectroscopy. By solving the time-dependent Schrödinger equation, we find one remarkable band gap emission besides the normal high harmonics generated in the interaction of a mid-infrared laser pulse and a semiconductor. It is shown that the band gap emission yield is directly connected to the population in the conduction band (CB). By adopting a pump-probe scheme, the time-dependent population in the CB, that is the dynamical Bloch oscillation, can be probed by measuring the band gap emission signal versus pump-probe delay. We also present a model based on accelerated Bloch states to explain the time-resolved measurement of dynamical Bloch oscillation.

1. Introduction

In solid-state physics, the oscillation dynamics of a Bloch electron in the presence of an electric field is a fundamental quantum-mechanical process [1–10]. The seminal works of Bloch [1] and Zener [2] on the dynamics of a Bloch electron in periodic potentials predicted that the quasi-momentum $\hbar\mathbf{k}$ of a Bloch electron in an electric field $\mathbf{F}$ follows the acceleration theorem $\hbar d\mathbf{k}/dt = -e\mathbf{F}$, where $\hbar$ is the reduced Planck constant and e is the elementary charge. As soon as the Bloch electron reaches a boundary of the Brillouin zone for a large enough $\mathbf{k}$, it is Bragg reflected as a consequence of the crystal symmetry. This phenomenon is known as Bloch oscillation (BO), where the electron moves periodically in real and reciprocal spaces.

Bloch oscillation is a basic dynamical process in semiconductors and is combined with many other phenomena of ultrafast charge transport [8–18]. A direct real-time observation of Bloch oscillations in semiconductors is crucial for understanding and studying these phenomena, which has so far only been realized in artificial superlattices [19–21]. However, the access to natural solids is often not available, because the Bloch frequency needs to be large enough to allow for full oscillations of the Bloch electron within the relevant scattering and tunneling times. For many years, it has been a common sense that Bloch oscillations can never be observed in bulk semiconductors, as witnessed by Kroemer's statement in his Nobel Prize autobiography [22]. The situation has recently changed due to the advent of state-of-the-art intense ultrashort pulses, in particular in previously inaccessible spectral regions such as the mid-infrared (MIR) and terahertz (THz). These pulses can serve as a desirable bias field in semiconductor because their photon energies are far below typical electronic interband transitions and their high intensity provides a strong bias. The oscillation driven by these intense pulses has a large enough Bloch frequency and can be maintained for more than one cycle within the scattering and tunneling

#334198 https://doi.org/10.1364/OE.26.023844
Journal © 2018 Received 1 Jun 2018; revised 16 Aug 2018; accepted 16 Aug 2018; published 30 Aug 2018

Optics EXPRESS

times. Recent experiments [16] have observed indirect signatures of Bloch oscillations in high harmonic generation by using a THz source. Nevertheless, a full oscillation of the Bloch electron in the semiconductor takes only a few or tens of femtoseconds and thus it is still a big challenge to realize the direct real-time measurement.

In this work, we propose time-resolved band gap emission spectroscopy to probe the dynamics of Bloch electrons in a semiconductor. By adopting an ultrashort 400 nm pump pulse and a MIR or THz probe pulse, which is a solid-state analog to the attosecond-streaking camera [23, 24], we can probe the dynamical Bloch oscillation in real time. The Bloch electron is shown to move with the rate $\hbar d\mathbf{k}/dt = -e\mathbf{F}$. In an intense THz field, the electrons are driven beyond the Brillouin zone boundary and Bragg reflection can occur. These results are explained by our theoretical model for the pump-probe scheme by using the accelerated Bloch states.

2. Method

Our simulation is performed by solving the single-active electron time-dependent Schrödinger equation (TDSE) [25–28], in which we describe the laser-crystal interaction in a one-dimensional system with the laser field polarized in the crystal plane. Since the wavelengths we are interested in are much larger than the lattice constant, the dipole approximation is employed. In the length gauge, the time-dependent Hamiltonian is written as (atomic units are used unless otherwise stated)

$$\hat{H}(t) = \hat{H}_0 + xF(t) \tag{1}$$

where $\hat{H}_0 = \frac{\hat{p}^2}{2} + V(x)$ is the field-free Hamiltonian and $F(t)$ is the electric field of the driving laser. $\hat{p}$ is the momentum operator and $V(x)$ is the periodic lattice potential. In our calculations, we choose the Mathieu-type potential [29] $V(x) = -V_0[1 + \cos(2\pi x/a_0)]$ with $V_0 = 0.37$ a.u. and lattice constant $a_0 = 8$ a.u.. In the absence of an external laser field, the eigenvalue equation of the field-free Hamiltonian $\hat{H}_0$ can be written as

$$\hat{H}_0\phi_n(x) = E_n\phi_n(x). \tag{2}$$

The eigenenergies E_n and the eigenstates $\phi_n(x)$ can be obtained by solving for the eigenvalues and eigenvectors of $\hat{H}_0$ on a coordinate grid.

The obtained eigenvalues versus the eigenstate number are shown in Fig. 1(a). The valence band (VB) and conduction band (CB) can be clearly distinguished. The energy gap between VB and CB is $E_g = 4.2$ eV, which mimics that of a direct semiconductor. Note that the other bands are also calculated but not plotted here. We also calculate the energy bands by the Bloch-state expansion in k-space [25, 26]. The results are shown in Fig. 1(b). Comparing the energy bands in Fig. 1(a) and 1(b), one can see that the number of bands, the width of the bands and the band gaps agree well with each other. Therefore, we can also discuss the oscillation of a Bloch electron in eigenstate number space.

With the interaction of laser field, the time-dependent wavefunction $\Psi(x, t)$ is obtained by solving the TDSE with the split-operator technique [30, 31]. The initial state is located at the top of the VB. A Gaussian envelope is adopted for all laser pulses in this work. The harmonic spectrum is obtained by calculating the Fourier transform of the laser-induced dipole acceleration:

$$S(\omega) = |\int a(t)e^{i\omega t}dt|^2 \tag{3}$$

where the laser induced dipole acceleration is

$$a(t) = \langle\Psi(x, t)| - \partial_x V|\Psi(x, t)\rangle. \tag{4}$$

Optics EXPRESS

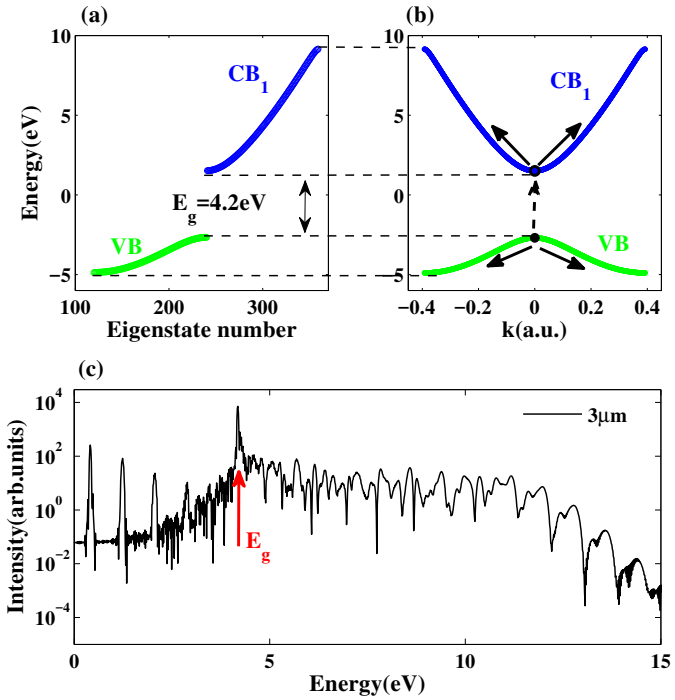

Fig. 1. (a) and (b) are the band structures calculated by the diagonalization scheme in coordinate space and by the Bloch-state expansion in reciprocal space, respectively. (c) The harmonic spectrum for laser wavelength $\lambda = 3\mu$m and intensity $I = 8 \times 10^{11}$ W/cm^2. The arrow indicates the band gap E_g.

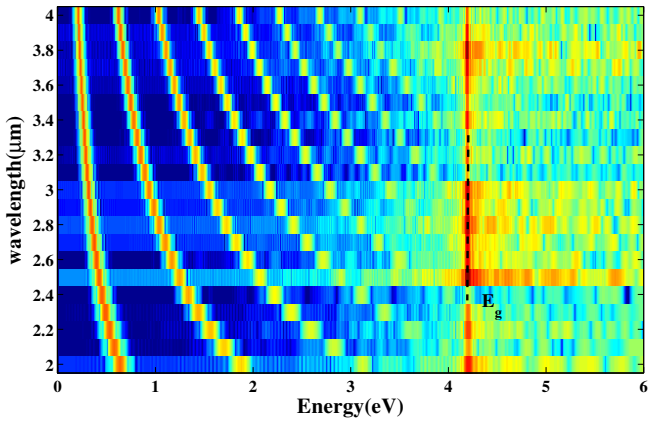

Fig. 2. Harmonic spectra for laser wavelengths from $\lambda = 2\mu$m to 4μm and intensity $I = 8 \times 10^{11}$W/cm^2. The dashed line indicates the band gap E_g.

Optics EXPRESS

3. Results and discussions

Figure 1(c) shows the calculated harmonic spectrum by using a laser pulse with wavelength $\lambda = 3$ μm and intensity $I = 8 \times 10^{11}$ W/cm^2. The full width at half maximum (FWHM) of the Gaussian envelope is 4 T_0, where T_0 denotes the optical cycle of the laser pulse. As is shown in Fig. 1(c), the harmonic spectrum exhibits a fast decay with clear odd harmonics in the low-energy region and a plateau structure. These results agree with previous work [25]. Besides the normal high harmonic signal, the harmonic spectrum shows a remarkable peak near 4.2 eV, which equals to the band gap energy between the VB and CB. Hereafter, we call this signal band gap emission.

We also perform the simulation by changing the laser wavelength λ from 2 μm to 4 μm. The results are shown in Fig. 2. The simulation shows that the central frequency of the remarkable peak remains at 4.2 eV irrespective of the change of the laser parameters (the simulations with different laser intensity and pulse duration are also performed but the results are not shown here). Note that one can also see a similar peak in the experiment performed on a ZnO crystal [8], which was called fluorescence signal in [8] but has not attracted much attention so far.

In order to get an intuitive insight of the band gap emission signal, we analyze the sub-cycle dynamics of the emission process with the time-frequency spectrum and time-dependent population imaging [32, 33]. The time-frequency spectrum is calculated by the Gabor transform [34, 35]. The time-dependent population imaging is calculated by $|\langle\phi_n(x)|\Psi(x,t)\rangle|^2$. In Fig. 3(a) and 3(b), we plot the vector potential $|A(t)| = |\int_{-\infty}^{t} F(\tau)d\tau|$ and the time-dependent population in the CB, respectively. One can see that the population oscillates following the vector potential. The electron momenta are driven from zero up to their maximum value and back to zero in every half cycle of the driving field. This corresponds to the laser-driven oscillation of Bloch electrons in reciprocal space, i.e., the so-called dynamical Bloch oscillation [16]. Note that the population oscillation, which is termed the field-induced transient population [9], can lead to the oscillation of the transient observable [9, 36–38]. After the laser pulse is gone, a fractional population survives at the bottom of CB. For clarity, we call it real population. This population results from resonances that exist in the laser dressed band gap resulting in conduction band population that grows through the duration of the pulse [39, 40]. In Fig. 3(c), we plot the time-frequency spectrum. The horizontal dashed line marks the energy of the band gap emission signal at 4.2 eV. As is shown in Fig. 3(c), the emission time of band gap signal is continuously maintained after 5 T_0 when the population is mainly located at the bottom of the CB. Unlike the harmonics, the band gap emission signal is a long-lived signal, which is dominantly emitted at the tail of the laser pulse and even after the laser pulse is gone. On the contrary, we also performed simulation using a laser pulse with a sine square envelope without long enough evolution time. The band gap emission signal is significantly suppressed as that in [41]. The comparison between Fig. 3(b) and 3(c) indicate that the band gap signal is directly connected to the real population at the bottom of the CB.

According to the discussion above, one can employ the band gap emission signal as a probe of the population oscillation, that is the dynamical Bloch oscillation driven by the pump pulse. To this end, we propose a time-resolved band gap emission spectroscopy experiment by adopting a pump-probe scheme. The Bloch electron oscillates in the long-wavelength MIR pump pulse. The pump pulse has a low intensity, thus the excitation from the VB to the CB can be ignored. An ultrashort violet (e.g., 400 nm) probe pulse is employed to excite the electron from the VB to the CB. The pulse duration of the probe pulse needs to be much shorter than the optical cycle of the pump pulse. In this scheme, the probe pulse triggers the dynamical Bloch oscillation. By detecting the band gap emission yield as a function of pump-probe delay, one can probe the dynamical Bloch oscillation in real time.

To show how one can extract the dynamical Bloch oscillation, we consider to model the electron dynamics in the above scheme in an intuitive picture. Following Refs. [42, 43], we adopt the accelerated Bloch states (the eigenstates of the time-dependent Hamiltonian) as a basis to

Optics EXPRESS

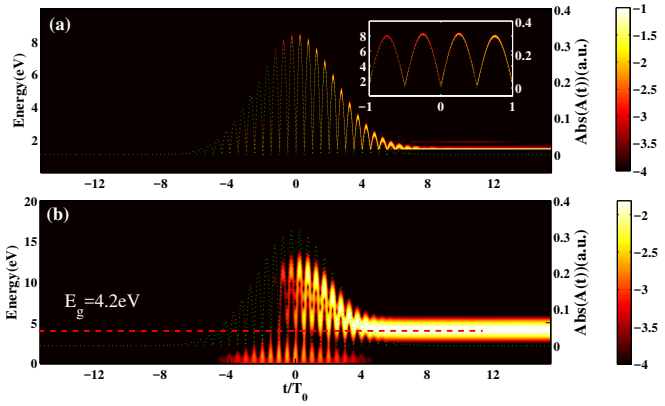

Fig. 3. (a) The time-dependent population imaging picture of the conduction band CB. The insert shows a zoom in of the result at peak of the laser pulse. The colorbar marks the population on a logarithmic scale. (b)The time-frequency harmonic spectrum obtained for a laser wavelength $\lambda = 3\mu$m. The colorbar marks the harmonic yield on a logarithmic scale. The green dashed lines mark the absolute value of the vector potential $|\mathbf{A}(t)|$.

solve the TDSE,

$$\psi_{k_0}(r,t) = \sum_m \alpha_{m,k_0}(t) e^{-i\int_{t_0}^{t} d\tau E_m(k(\tau))} \varphi_{m,k_0}(r,t) \tag{5}$$

where the accelerated Bloch states are $\varphi_{m,k_0}(r,t) = e^{-iA(t)r}\chi_{m,k(t)}(r)$, and the time-dependent crystal momentum is $k(t) = k_0 + A(t)$. $\chi_{m,k}(r)$ is a Bloch state with a band index m and a crystal momentum k. The Hamiltonian can be divided into three parts:

$$\hat{H}(t) = \begin{cases} \frac{[\hat{p}+A_{Pp}]^2}{2} + V(r) & t = (-\infty, \Delta t - \frac{\delta t}{2}) \\ \frac{[\hat{p}+A_{Pp}+A_{Pb}]^2}{2} + V(r) & t = [\Delta t - \frac{\delta t}{2}, \Delta t + \frac{\delta t}{2}] \\ \frac{[\hat{p}+A_{Pp}]^2}{2} + V(r) & t = (\Delta t + \frac{\delta t}{2}, \infty) \end{cases} \tag{6}$$

where A_{Pp} and A_{Pb} are the vector potentials of the pump and probe pulses, respectively. We assume that the pump pulse is centered at $t = 0$ and the probe pulse is delayed by Δt. δt is the pulse duration of the probe pulse. Under the parameters we used in this work, the population in higher conduction bands are much lower (less than 1%) than that in the first conduction band. Therefore, only one VB and one CB are considered here and the initial state is chosen as $\chi_{\mathrm{VB},0}(r)$. In the time range of $t = (-\infty, \Delta t - \frac{\delta t}{2})$ and $t = (\Delta t + \frac{\delta t}{2}, \infty)$, only the pump pulse is turned on and the transition between VB and CB can be ignored. In the time range of $t = [\Delta t - \frac{\delta t}{2}, \Delta t + \frac{\delta t}{2}]$, the probe pulse excites the Bloch electron. Since the probe pulse duration is extremely short ($\delta t \ll T_0$), we can only consider the transition between VB and CB but ignore the oscillation of the Bloch electron in $[\Delta t - \delta t/2, \Delta t + \delta t/2]$. Therefore, the solution of TDSE can be expressed as

$$\psi(r,t) = \begin{cases} \alpha_{\mathrm{VB}}(t) e^{-i\int_{-\infty}^{t} d\tau E_{\mathrm{VB}}(k(\tau))} \varphi_{\mathrm{VB}}(r,t) & t = (-\infty, \Delta t - \frac{\delta t}{2}) \\ \sum_{m=\mathrm{VB,CB}} \alpha_m(\Delta t) e^{-i\int_{-\infty}^{\Delta t} d\tau E_m(k(\tau))} \varphi_m(r,\Delta t) & t = [\Delta t - \frac{\delta t}{2}, \Delta t + \frac{\delta t}{2}] \\ \sum_{m=\mathrm{VB,CB}} \alpha_m(t) e^{-i\int_{-\infty}^{t} d\tau E_m(k(\tau))} \varphi_m(r,t) & t = (\Delta t + \frac{\delta t}{2}, \infty) \end{cases} \tag{7}$$

For $t < \Delta t$, $\alpha_{\mathrm{VB}}(t) = 1$ and $\alpha_{\mathrm{CB}}(t) = 0$. For $t > \Delta t$, $\alpha_{\mathrm{VB}}(t) = 1 - \alpha_{\mathrm{CB}}(t)$ and $\alpha_{\mathrm{CB}}(t) = \alpha_{\mathrm{CB}}(\Delta t) \propto d_{vc}(k(\Delta t))$, where $d_{vc}(k) = \langle \chi_{\mathrm{VB},k}|r|\chi_{\mathrm{CB},k}\rangle$. In this case, the radiation yield is

Optics EXPRESS

$$S(\omega) \propto \left| \int \langle \psi | r | \psi \rangle e^{i\omega t} dt \right|^2$$
$$= \left| \int dt e^{i\omega t} \sum_{m=\mathrm{VB,CB}} \sum_{n=\mathrm{VB,CB}} \alpha_m^*(t)\alpha_n(t) e^{-i\int_{-T}^{t} d\tau E_{nm}(k(\tau))} d_{nm}(k(t)) \right|^2. \quad (8)$$

One can see that only the terms satisfying $E_{nm}(k) = E_n(k) - E_m(k) = E_g$ contribute to the signal at the band edge $S(\omega = E_g)$. Then the emission yield can be obtained

$$S(\omega = E_g) \propto \int dt |\alpha_{\mathrm{VB}}^*(t)\alpha_{\mathrm{CB}}(t) d_{vc}(k(t))\delta(k(t) - 0)|^2. \quad (9)$$

We can assume that the depletion of the VB due to the THz field can be ignored, i.e., $|\alpha_{\mathrm{VB}}(t)|^2 \approx 1$, as in the well-known Lewenstein model [44] for HHG in a gas medium. Then, we have

$$S(\omega = E_g) \propto \int dt N_{\mathrm{CB},0}(t) |d_{vc}(0)|^2 \quad (10)$$

where $N_{\mathrm{CB},0}(t) = |\alpha_{\mathrm{CB}}(t)\delta(k(t)-0)|^2$ is the population at the bottom of the CB. Therefore, the band gap emission signal is proportional to the integration of the transition dipole and the population at the bottom of the CB. Note that $d_{vc}(0)$ is a constant and $\alpha_{\mathrm{CB}}(t) = \alpha_{\mathrm{CB}}(\Delta t) \propto d_{vc}(k(\Delta t))$, the delay time dependence of the band gap signal can be rewritten as

$$S(\omega = E_g, \Delta t) \propto N_{\mathrm{CB},0}(t) \propto |d_{vc}(k(\Delta t))|^2. \quad (11)$$

The parameter $k(\Delta t)$ is the location of the Bloch electron at the time Δt in the pump pulse. The population at the bottom of the CB is proportional to the term $|d_{vc}(k(\Delta t))|^2$, which contains the information of $k(\Delta t)$. By scanning the delay time Δt, one can probe the population at the bottom of the CB by the band gap emission yield, which tracks the oscillation of the Bloch electron.

To demonstrate the above scheme, we calculate the band gap signal as a function of pump-probe delay by numerically solving the TDSE. In our proposed experimental scheme, we are not creating large carrier densities that would lead to rapid dephasing via carrier scattering. As the Bloch oscillation period is therefore much shorter than the dephasing time in our scheme, we can neglect dephasing in this work. The wavelengths of the pump and probe pulses are 3.0 μm and 400 nm, respectively, which can be realized by an optical parameter amplifier and second-harmonic generation pumped by the fundamental Ti:Sapphire laser. The duration of the pump pulse is about 20 fs and the pump pulse intensity is 8×10^9 W/cm^2. The duration of the probe pulse is 2 fs and the intensity is 8×10^{10} W/cm^2. Figure 4(a) shows the time-dependent population imaging in the CB. Figure 4(b) shows the band gap emission yield as a function of pump-probe delay. One can see that both the CB population and the band gap signal oscillate following the vector potential of the pump pulse with the period of $T_0/2$. The result agrees well with the acceleration theorem. However, by comparing Fig. 4(a) to 4(b) the oscillation phases of the CB population and band gap emission differ by $\pi/2$. In other words, the CB population reaches the highest energy state at $\frac{2n+1}{4} T_0$, when the band gap emission yield is minimum. This can be well explained by Eq. (11). When $\Delta t = \frac{2n+1}{4} T_0$, the Bloch electron is driven farthest away from the initial state where $k = 0$ a.u. and $d_{vc}(k(\Delta t))$ is smallest, leading to a minimum of the band gap signal. When $\Delta t = \frac{n}{2} T_0$, the Bloch electron is dominantly populated at the state of $k = 0$ a.u. where $d_{vc}(k(\Delta t))$ is largest and therefore the band gap emission becomes maximum.

In a typical wide band gap semiconductor, the VB is fully occupied initially. To consider this effect, we perform the calculation by taking into account the initially fully occupied VB with the model described in [45]. For a detailed description of the formalism, we refer the reader to [45].

Optics EXPRESS

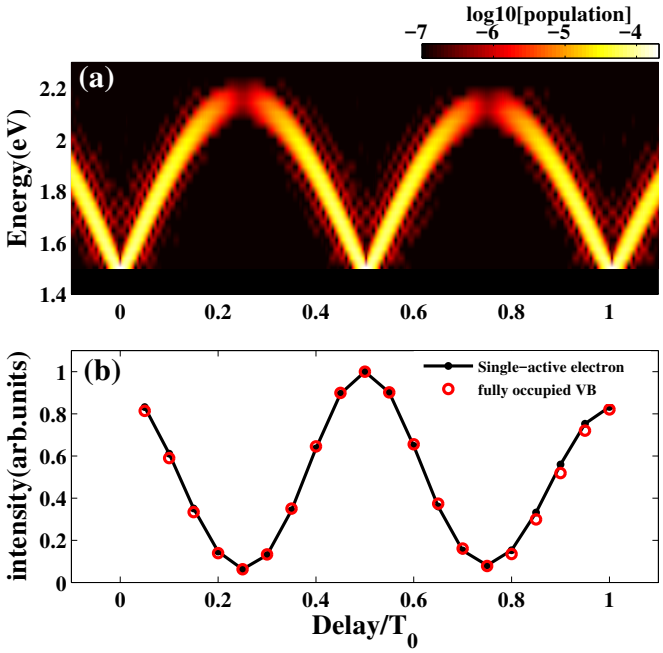

Fig. 4. The time-dependent population imaging picture (a) and the delay-dependent band gap signal (b) for $\lambda = 3$ μm. The solid line is obtained by TDSE with single-active electron. The circles is obtained by TDSE with fully occupied VB.

Briefly, we adopt the eigenstates with different k values in the VB (see Fig. 1(b)) as the initial state and then obtain the time-dependent wavefunction and also laser-induced dipole acceleration by numerically solving the TDSE for each initial state. The total dipole acceleration is calculated by coherent summation over the initial states for all the k in the VB. Then the spectrum of the radiation is calculated by Fourier transforming dipole acceleration. The delay-time-dependent band gap signal is shown by the circles in Fig. 4(b). One can see that the results are in good agreement with simulation with single-active electron TDSE model. This is because the excitation probability decreases quickly with increasing the energy gap between the CB and VB. The energy gap is smallest at $k = 0$ a.u., i.e., the top of the VB. Therefore, only a small portion of the electrons populated near $k = 0$ a.u. are excited to the CB under the laser conditions in this work. Then the TDSE model with a single-active electron at $k = 0$ a.u. still can reliably reproduce the simulation with the fully occupied VB.

So far, we have shown that one can trace the oscillation of Bloch electron with our pump-probe scheme. Note that the maximum electron momentum is determined by the maximum of the vector potential of the pump pulse. Under the pump intensity and wavelength considered in Fig. 4(a), the maximum energy populated in the CB is 2.2 eV, which is smaller than the width of the CB (9.2 eV as shown in Fig. 1). Therefore, the oscillation of Bloch electron stays far away from the Brillouin zone boundaries and no Bragg reflection can be observed. To detect the full Bloch oscillation, we next consider to use a THz pump pulse with the central wavelength of 40 μm (corresponds to 7.5 THz). The pump pulse intensity is increased to 2×10^{10} W/cm^2. The probe pulse intensity is increased to 4×10^{11} W/cm^2 accordingly. Figures 5(a) and 5(b) show the time-dependent CB population and the band gap emission yield as a function of pump-probe delay. In contrast to the results in Fig. 4, the vector potential of the THz pump pulse is large enough to drive the electron to 9.2 eV, reaching the edge of the Brillouin zone. As shown in

Optics EXPRESS

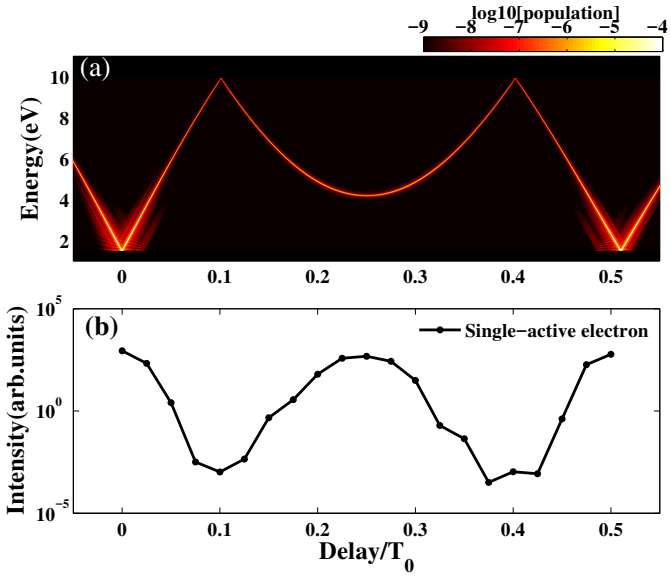

Fig. 5. The time-dependent population imaging picture (a) and the delay-dependent band gap signal (b) for $\lambda = 40$ μm. The solid line is obtained by TDSE with single-active electron.

Fig. 5(a), the Bloch electrons are driven from zero up to their maximum. Then, at 0.1 T_0, the electron momentum changes its sign, once Bragg reflection occurs. As shown in Fig. 5(b), these phenomena can all be monitored by observing the delay-dependent band gap emission yield.

4. Conclusion

In conclusion, we proposed a time-resolved band gap emission spectroscopy scheme to probe the dynamical Bloch oscillation in real time. It is shown that a remarkable band gap emission can be generated besides the normal high harmonics in the interaction of a mid-infrared laser pulse and a semiconductor. By adopting an ultrashort probe pulse and MIR or THz pump pulse, one can trace the dynamics of Bloch electrons in real time by monitoring the band gap signal versus pump-probe delay. This scheme suggests an all-optical method for directly investigating the ultrafast dynamics of electrons in semiconductors.

Funding

National Natural Science Foundation of China (NSFC) (11874165,11627809, 11774109, and 11704137), the program for HUST Academic Frontier Youth Team, and Deutsche Forschungsgemeinschaft priority program QUTIF (SPP1840 SOLSTICE).

References and links

1. F. Bloch, "Über die Quantenmechanik der Elektronen in Kristallgittern," Z. Phys. **52**, 555 (1929).
2. C. Zener, "A theory of the electrical breakdown of solid dielectrics," Proc. R. Soc. A **145**, 523 (1934).
3. A. Leitenstorfer, S. Hunsche, J. Shah, M. C. Nuss, and W. H. Knox, "Femtosecond charge transport in polar semiconductors," Phys. Rev. Lett. **82**, 5140 (1999).
4. W. Kuehn, P. Gaal, K. Reimann, M. Woerner, T. Elsaesser, and R. Hey, "Coherent ballistic motion of electrons in a periodic potential," Phys. Rev. Lett. **104**, 146602 (2010).
5. D. Golde, T. Meier, and S. W. Koch, "High harmonics generated in semiconductor nanostructures by the coupled dynamics of optical inter- and intraband excitations," Phys. Rev. B **77**, 075330 (2008).
6. D. Golde, M. Kira, T. Meier, and S. W. Koch, "Microscopic theory of the extremely nonlinear terahertz response of semiconductors," Phys. Status Solidi B **248**, 863 (2011).

Optics EXPRESS

7. T. Higuchi, C. Heide, K. Ullmann, H. B. Weber, and P. Hommelhoff, "Light-field-driven currents in graphene," Nature **550**, 224 (2017).
8. S. Ghimire, A. D. DiChiara, E. Sistrunk, P. Agostini, L. F. DiMauro, and D. A. Reis, "Observation of high-order harmonic generation in a bulk crystal," Nat. Phys. **7**, 138 (2011).
9. A. Schiffrin, T. Paasch-Colberg, N. Karpowicz, V. Apalkov, D. Gerster, S. Mühlbrandt, M. Korbman, J. Reichert, M. Schultze, S. Holzner, J. V. Barth, R. Kienberger, R. Ernstorfer, V. S. Yakovlev, M. I. Stockman, and F. Krausz, "Optical-field-induced current in dielectrics," Nature **493**, 70 (2013).
10. O. D. Mücke, "Isolated high-order harmonics pulse from two-color-driven Bloch oscillations in bulk semiconductors," Phys. Rev. B **84**, 081202(R) (2011).
11. H. Xie, M. Li, S. Luo, Y. Li, J. Tan, Y. Zhou, W. Cao, and P. Lu, "Photoelectron holography and forward scattering in atomic ionization by elliptically polarized laser pulses," Opt. Lett. **43**, 3220 (2018).
12. B. Wang, L. He, F. Wang, H. Yuan, X. Zhu, P. Lan, and P. Lu, "Resonance-modulated wavelength scaling of high-order-harmonic generation from H_2^+," Phys. Rev. A **97**, 013417 (2018).
13. C. Schmidt, J. Bühler, A. C. Heinrich, J. Allerbeck, R. Podzimski, D. Berghoff, T. Meier, W. G. Schmidt, C. Reichl, W. Wegscheider, D. Brida and A. Leitenstorfer, "Signatures of transient Wannier-Stark localization in bulk gallium arsenide," Nat. Commun. **9**, 2890 (2018).
14. S. Ghimire, A. D. DiChiara, E. Sistrunk, G. Ndabashimiye, U. B. Szafruga, A. Mohammad, P. Agostini, L. F. DiMauro, and D. A. Reis, "Generation and propagation of high-order harmonics in crystals," Phys. Rev. A **85**, 043836 (2012).
15. S. Ghimire, A. D. DiChiara, E. Sistrunk, U. B. Szafruga, P. Agostini, L. F. DiMauro, and D. A. Reis, "Redshift in the optical absorption of ZnO single crystals in the presence of an intense midinfrared laser field," Phys. Rev. Lett. **107**, 167407 (2011).
16. O. Schubert, M. Hohenleutner, F. Langer, B. Urbanek, C. Lange, U. Huttner, D. Golde, T. Meier, M. Kira, ,S. W. Koch, and R. Huber, "Sub-cycle control of terahertz high-harmonic generation by dynamical Bloch oscillations," Nat. Photon. **8**, 119 (2014).
17. P. Földi, M. G. Benedict and V. S. Yakovlev, "The effect of dynamical Bloch oscillation on optical-field-induced current in a wide-gap dielectric," New J. Phys. 15, 063019 (2013).
18. C. R. McDonald, G. Vampa, P. B. Corkum and T. Brabec, "Interband Bloch oscillation mechanism for high-harmonic generation in semiconductor crystals," Phys. Rev. A 92, 033845 (2015).
19. F. Feldmann, K. Leo, J. Shah, D. A. B. Miller, J. E. Cunningham, T. Meier, G. von Plessen, A. Schulze, P. Thomas, and S. Schmitt-Rink, "Optical investigation of Bloch oscillations in a semiconductor superlattice," Phys. Rev. B **46**, 7252 (1992).
20. C. Waschke, H. G. Roskos, R. Schwedler, K. Leo, H. Kurz and K. Köhler, "Coherent submillimeter wave emission from Bloch oscillations in a semiconductor superlattice," Phys. Rev. Lett. **70**, 3319 (1993).
21. V. G. Lyssenko, G. Valušis, F. Löser, T. Hasche, K. Leo, M. M. Dignam, and K. Köhler, "Direct measurement of the spatial displacement of Bloch-oscillating electrons in semiconductor superlattices," Phys. Rev. Lett. **79**, 301 (1997).
22. "...it became obvious that the huge fields required for Bloch oscillations in a bulk semiconductor could never be reached." seen in https://www.nobelprize.org/nobel_prizes/physics/laureates/2000/kroemer-bio.html.
23. J. Itatani, F. Quéré, G. L. Yudin, M. Yu. Ivanov, F. Krausz, and P. B. Corkum, "Attosecond streak camera," Phys. Rev. Lett. **88**, 173903 (2002).
24. M. Kitzler, N. Milosevic, A. Scrinzi, F. Krausz, and T. Brabec, "Quantum theory of attosecond XUV pulse measurement by laser dressed photoionization," Phys. Rev. Lett. **88**, 173904 (2002).
25. M. Wu, S. Ghimire, D. A. Reis, K. J. Schafer, and M. B. Gaarde, "High-harmonic generation from Bloch electrons in solids," Phys. Rev. A **91**, 043839 (2015).
26. T. Y. Du, and X. B. Bian, "Quasi-classical analysis of the dynamics of the high-order harmonic generation from solids," Opt. Express **25**, 151 (2017).
27. M. He, Y. Li, Y. Zhou, M. Li, W. Cao, and P. Lu, "Direct visualization of valence electron motion using strong-field photoelectron holography," Phys. Rev. Lett. **120**, 133204 (2018).
28. C. Zhai, X. Zhang, X. Zhu, L. He, Y. Zhang, B. Wang, Q. Zhang, P. Lan, and P. Lu, "Single-shot molecular orbital tomography with orthogonal two-color fields," Opt. Express **26**, 2775 (2018).
29. J. C. Slater, "A soluble problem in energy bands," Phys. Rev. **87**, 807 (1952).
30. M. D. Feit, J. A. Fleck, Jr., and A. Steiger, "Solution of the Schrödinger equation by a spectral method," J. Comput. Phys. **47**, 412 (1982).
31. L. Li, P. Lan, L. He, X. Zhu, J. Chen, and P. Lu, "Scaling law of high harmonic generation in the framework of photon channels," Phys. Rev. Lett. **120** 223203 (2018).
32. X. Liu, X. Zhu, P. Lan, X. Zhang, D. Wang, Q. Zhang, and P. Lu, "Time-dependent population imaging for high-order-harmonic generation in solids," Phys. Rev. A **95**, 063419 (2017).
33. L. He, Q. Zhang, P. Lan, W. Cao, X. Zhu, C. Zhai, F. Wang, W. Shi, M. Li, X. Bian, P. Lu, and A. D. Bandrauk, "Monitoring ultrafast vibrational dynamics of isotopic molecules with frequency modulation of high-order harmonics," Nat. Commun. **9**, 1108 (2018).
34. D. Gabor, "Theory of communication. Part 1: The analysis of information," J. Inst. Electr. Eng. **93**, 429 (1946).
35. C. C. Chirilă, I. Dreissigacker, E. V. van der Zwan, and M. Lein, "Emission times in high-order harmonic generation," Phys. Rev. A **81**, 033412 (2010).

Optics EXPRESS

36. M. Schultze, E. M. Bothschafter, A. Sommer, S. Holzner, W. Schweinberger, M. Fiess, M. Hofstetter, R. Kienberger, V. Apalkov, V. S. Yakovlev, M. I. Stockman, and F. Krausz, "Controlling dielectrics with the electric field of light," Nature **493**, 75 (2013).
37. N. Tancogne-Dejean, O. D. Mücke, F. X. Kärtner, and A. Rubio, "Ellipticity dependence of high-harmonic generation in solids originating from coupled intraband and interband dynamics," Nat. Commun. **8**, 745 (2017).
38. F. Krausz, and M. I. Stockman, "Attosecond metrology: from electron capture to future signal processing," Nat. Photon. **8**, 205 (2014).
39. V. E. Gruzdev, "Photoionization rate in wide band-gap crystals," Phys. Rev. B **75**, 205106 (2007).
40. C. R. McDonald, G. Vampa, P. B. Corkum, and T. Brabec, "Intense laser solid state physics: unraveling the difference between semiconductors and dielectrics," Phys. Rev. Lett. **118**, 173601 (2017).
41. G. Vampa, C. R. McDonald, G. Orlando, D. D. Klug, P. B. Corkum, and T. Brabec, "Theoretical analysis of high harmonic generation in solids," Phys. Rev. Lett. **113**, 073901 (2014).
42. V. Yakovlev, S. Kruchinin, T. Paasch-Colberg, M. Stockman, and F. Krausz, *Ultrafast Dynamics Driven by Intense Light Pulses*, edited by M. Kitzler, S. Gräfe (Springer Series on Atomic, Optical, and Plasma Physics, 2016), p. 295-315.
43. S. Y. Kruchinin, F. Krausz, and V. S. Yakovlev, "Colloquium: Strong-field phenomena in periodic systems," Rev. Mod. Phys. **90**, 021002 (2018).
44. M. Lewenstein, P. Balcou, M. Y. Ivanov, A. L'Huillier, and P. B. Corkum, "Theory of high-harmonic generation by low-frequency laser fields," Phys. Rev. A **49**, 2117 (1994).
45. T. Ikemachi, Y. Shinohara, T. Sato, J. Yumoto, M. Kuwata-Gonokami, and K. L. Ishikawa, "Trajectory analysis of high-order-harmonic generation from periodic crystal," Phys. Rev. A **95**, 043416 (2017).